

Roles of Potential Gradient and Electrode Bandwidth on Negative Differential Resistance in One-Dimensional Band Insulator

Yasuhiro Tanaka^{1,2*} and Kenji Yonemitsu^{1,2}

¹*Department of Physics, Chuo University, Bunkyo, Tokyo 112-8551, Japan*

²*JST, CREST, Chiyoda, Tokyo 102-0076, Japan*

A negative differential resistance (NDR) in a one-dimensional band insulator attached to electrodes is investigated. We systematically examine the effects of an electrode bandwidth and a potential distribution inside the insulator on current-voltage characteristics. We show that, in uncorrelated systems, the NDR is generally caused by a linear potential gradient as well as by a finite electrode bandwidth. In particular, the former reduces the effective bandwidth of the insulator for elastic tunneling by tilting its energy band, so that it brings about the NDR even in the limit of large electrode bandwidth.

1. Introduction

Recently, nonlinear conduction phenomena in low-dimensional electron systems such as Mott insulators^{1,2} and charge-ordered materials³ have been intensively studied. In theoretical investigations, several authors consider a model structure where an insulator with a length L_C in the central part is attached to the left and right ($\alpha = L, R$) electrodes.⁴⁻¹⁴ A schematic picture of the model for a one-dimensional case is shown in Fig. 1. When a bias voltage is applied, the electrode bandwidth and the electrode density of states are important factors for determining current-voltage (J - V) characteristics. In fact, the finite electrode bandwidth results in a negative differential resistance (NDR) if we consider only elastic electron tunneling for transport. This NDR, which is not related to the electron correlation, has been shown using a noninteracting resonant level model¹⁵ in which the central part consists of a single site ($L_C = 1$). When L_C becomes large, the potential distribution inside the central part is also important. It gives a spatial dependence of the electric field and affects the breakdown mechanism of insulators.¹² Although it is expected that the NDR depends on both the potential

distribution and the electrode degrees of freedom, their effects have not been examined so far for large- L_C systems.

2. Model and Method

In this paper, we study the J - V characteristics of a one-dimensional band insulator at half-filling, to which semi-infinite electrodes are attached (Fig. 1). We assume that electrons are noninteracting in both the central part and the electrodes. Although we do not consider insulators that are caused by electron-electron interactions here, some of our results will be qualitatively applied to such insulators at least on the mean-field level.¹² The total Hamiltonian is written as $H = H_L + H_R + H_C + H_{con}$ with

$$H_L = -t_E \sum_{i \leq 0, \sigma} (c_{i\sigma}^\dagger c_{i-1\sigma} + h.c.) + \mu_L \sum_{i \leq 0, \sigma} c_{i\sigma}^\dagger c_{i\sigma}, \quad (1)$$

$$H_R = -t_E \sum_{i \geq L_C+1, \sigma} (c_{i+1\sigma}^\dagger c_{i\sigma} + h.c.) + \mu_R \sum_{i \geq L_C+1, \sigma} c_{i\sigma}^\dagger c_{i\sigma}, \quad (2)$$

$$H_C = - \sum_{i=1, \sigma}^{L_C-1} [t + (-1)^{i+1} \delta t] (c_{i+1\sigma}^\dagger c_{i\sigma} + h.c.) + \sum_{i=1, \sigma}^{L_C} V_C(i) c_{i\sigma}^\dagger c_{i\sigma}, \quad (3)$$

$$H_{con} = -\tau \sum_{\sigma} (c_{0\sigma}^\dagger c_{1\sigma} + c_{L_C\sigma}^\dagger c_{L_C+1\sigma} + h.c.), \quad (4)$$

where H_α and H_C are the Hamiltonians for the electrode α and the central part, respectively, and H_{con} describes the coupling between them. $c_{i\sigma}^\dagger$ ($c_{i\sigma}$) denotes the creation (annihilation) operator for an electron with spin σ at the i th site, and $h.c.$ stands for hermitian conjugate. For the electrodes, the transfer integral is denoted by t_E and their coupling to the central part is denoted by τ . In Eq. (3), the transfer integral t has a modulation δt that gives a charge gap $\Delta = 4\delta t$. We use t as a unit of energy. In the following, the bandwidth of the central part (the electrodes) is written as W (W_E) where $W \simeq 4t$ if $t \gg \delta t$ holds, and $W_E = 4t_E$. All these quantities are summarized in Table I. Since we do not consider the work-function difference at the interfaces, we set $\mu_L = V/2$ ($\mu_R = -V/2$) for the chemical potential of the electrode L (R) when the bias V is applied. $V_C(i)$ is the site potential for which we consider two cases. They are written as

$$V_C(i) = V[1/2 - i/(L_C + 1)], \quad (5)$$

and

$$V_C(i) = 0. \quad (6)$$

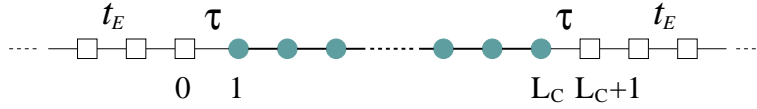


Fig. 1. (Color online) Schematic structure of the model. Left and right semi-infinite electrodes are connected by a one-dimensional band insulator. Solid (open) symbols represent the sites in the central part (electrodes).

Table I. Quantities that characterize our model. The independent parameters are δt , t_E , and τ .

Location	Quantity	Meaning
Central part	$t (= 1)$	Transfer integral
	$\Delta (= 4\delta t)$	Charge gap
	W	Bandwidth
Electrodes	t_E	Transfer integral
	W_E	Bandwidth
Interface	τ	Transfer integral between the central part and the electrodes

Table II. Conditions for calculations (i)-(iv) and calculation results for NDR.

Condition	Potential gradient	Electrode bandwidth	NDR
(i)	Present	Finite	Present
(ii)	Present	Infinite	Present
(iii)	Absent	Finite	Present
(iv)	Absent	Infinite	Absent

In Eq. (5), the central part has a linear potential gradient that corresponds to a uniform electric field; however, in the case of Eq. (6), there is no electric field: the voltage drop occurs only at the interfaces.

We use a nonequilibrium Green's function method¹⁶ in order to calculate the J - V curve, which can be carried out exactly since there are no electron-electron interactions in H . The retarded Green's function for the central part is written as

$$G^r(\epsilon) = [\epsilon \mathbf{1} - H_C - \Sigma_L^r(\epsilon) - \Sigma_R^r(\epsilon)]^{-1}, \quad (7)$$

where $\Sigma_\alpha^r(\epsilon)$ is the self-energy due to the electrode α and $\mathbf{1}$ is the unit matrix. The spin index is abbreviated. For the self-energies, the only nonzero matrix element is given by

$$[\Sigma_\alpha^r(\epsilon)]_{i_\alpha, i_\alpha} = \tau^2 [g_\alpha^r(\epsilon)]_{p_\alpha, p_\alpha}, \quad (8)$$

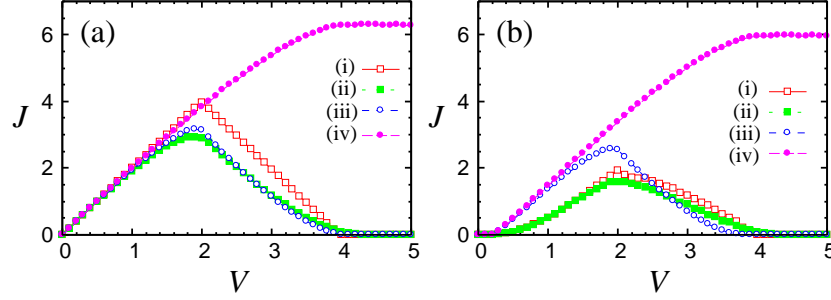


Fig. 2. (Color online) J - V characteristics with (a) $\delta t = 0$ and (b) $\delta t = 0.05$ obtained under the conditions (i)-(iv) that are described in the text and summarized in Table II. We use $t_E = \tau = 1$ and $L_C = 100$.

where $g_\alpha^r(\epsilon)$ is the Green's function of the isolated electrode α , i_L (i_R) is the leftmost (rightmost) site in the central part, and p_L (p_R) is the site adjacent to i_L (i_R) in the electrode L (R). We can obtain $[g_\alpha^r(\epsilon)]_{p_\alpha, p_\alpha}$ as

$$[g_\alpha^r(\epsilon)]_{p_\alpha, p_\alpha} = \begin{cases} \frac{\epsilon - \mu_\alpha}{2t_E^2} - \frac{i}{2t_E} \sqrt{4t_E^2 - (\epsilon - \mu_\alpha)^2} & (|\epsilon - \mu_\alpha| < 2t_E) \\ \frac{\epsilon - \mu_\alpha}{2t_E^2} - \text{sgn}(\epsilon - \mu_\alpha) \frac{1}{2t_E} \sqrt{4t_E^2 - (\epsilon - \mu_\alpha)^2} & (|\epsilon - \mu_\alpha| > 2t_E), \end{cases} \quad (9)$$

where $\text{sgn}(x) = 1$ [$\text{sgn}(x) = -1$] for $x > 0$ ($x < 0$) and we assume $t_E > 0$. If we introduce $\Gamma_\alpha(\epsilon) = -2\text{Im}[\Sigma_\alpha^r(\epsilon)]_{i_\alpha, i_\alpha}$ with $\Gamma_\alpha(\epsilon) = \frac{\tau^2}{t_E^2} \sqrt{4t_E^2 - (\epsilon - \mu_\alpha)^2} \theta(2t_E - |\epsilon - \mu_\alpha|)$, the current J is given by¹⁶

$$J = 2 \int_{\mu_R}^{\mu_L} d\epsilon \Gamma_L(\epsilon) \Gamma_R(\epsilon) |[G^r(\epsilon)]_{1, L_C}|^2, \quad (10)$$

where we set $e = h = 1$. When we compute J , an assumption that the electrode bandwidth W_E is much larger than the other energy scales is sometimes used. This is called the wide-band limit (WBL). In such a case, the self-energy is independent of energy and is reduced to $[\Sigma_\alpha^r(\epsilon)]_{i_\alpha, i_\alpha} = -i\Gamma_0/2$ with $\Gamma_0 = 2\tau^2/t_E$.¹⁷

3. Results

In order to elucidate the roles of the potential gradient and the electrode bandwidth, in the following, we use four conditions (i)-(iv) in the calculations, as summarized in Table II, depending on $V_C(i)$ and on whether the WBL is applied: $V_C(i)$ is given by Eq. (5) [Eq. (6)] in (i) and (ii) [(iii) and (iv)], and the WBL is used in (ii) and (iv). We show the J - V curves for $\delta t = 0$ and $\delta t = 0.05$ in Figs. 2(a) and 2(b), respectively, where we use $t_E = \tau = 1$ and $L_C = 100$. Although the cases (i) and (ii) for $\delta t = 0$ and the cases (iii) and (iv) for $\delta t = 0.05$ involve an artificial voltage drop in the central part, we show their

results for comparison. When $\delta t = 0$, the central part is a noninteracting metal, so that J shows a linear increase for small values of V . This feature appears regardless of the electrode bandwidth and $V_C(i)$. The slope in the linear regime is 2, which corresponds to the Landauer formula $G = \frac{2e^2}{h}T$ with the transmission probability $T = 1$. When the central part is a band insulator ($\delta t = 0.05$), the behavior of the J - V curves in the small- V region is different from that for $\delta t = 0$ because of the charge gap Δ . Moreover, it depends on $V_C(i)$. In (i) and (ii), the current is described by $J \sim V e^{-V_{\text{th}}/V}$ indicating the Landau-Zener (LZ) breakdown^{18,19} of the insulator; however, $J = 0$ for $V < \Delta = 0.2$ and it begins to increase at $V = \Delta$ in (iii) and (iv). These different behaviors depend on whether the electric field exists in the central part, as discussed in Ref. 12.

When V is large, the J - V curves for the metal and the band insulator are qualitatively similar. For (i)-(iii), the NDR occurs for $V \gtrsim 2$, whereas J monotonically increases and saturates at $V \simeq 4$ in (iv). There are two different sources of these NDRs. One is a finite electrode bandwidth, which has been discussed in the resonant level model.¹⁵ When V exceeds $W_E/2$, the energy window in which elastic tunneling is allowed diminishes so that the NDR occurs. The other origin is the potential $V_C(i)$ in Eq. (5). As discussed below, this results in a tilting of the band in the central part, which reduces the bandwidth for the elastic transport effectively (see the inset of Fig. 3). In (i), both factors give the NDR. In (ii), the potential gradient leads to the NDR, although the effect of the finite electrode bandwidth is absent because of the WBL. Since there is no electric field in the central part in (iii) and (iv), the NDR appears only when the electrode bandwidth is finite, which is basically the same as that in the resonant level model.¹⁵ These results are summarized in Table II.

Next, we discuss the above origins of the NDR from the energy dependence of the integrand in Eq. (10). In Fig. 3, we show $\Gamma_L(\epsilon)$, $\Gamma_R(\epsilon)$, $|G_{1,L_C}(\epsilon)|^2$, and $T(\epsilon) = \Gamma_L(\epsilon)\Gamma_R(\epsilon)|G_{1,L_C}(\epsilon)|^2$ as a function of ϵ for several values of V in the case of (i). $T(\epsilon)$ is plotted only in the region $\mu_R = -V/2 < \epsilon < \mu_L = V/2$. The functions $\Gamma_L(\epsilon)$ and $\Gamma_R(\epsilon)$ are identical for $V = 0$. When we increase V , the bands of the left and right electrodes shift in opposite directions, as shown in the inset of Fig. 3. Accordingly, the region $\epsilon_L < \epsilon < \epsilon_R$ in which $\Gamma_L(\epsilon)\Gamma_R(\epsilon)$ is finite decreases, where $\epsilon_L = -2t_E + \mu_L$ ($\epsilon_R = 2t_E + \mu_R$) is the energy of the band bottom (top) of the left (right) electrode. When V is small, $|G_{1,L_C}(\epsilon)|^2$ is suppressed at around $\epsilon = 0$ owing to the charge gap. This feature gradually disappears with increasing V . $|G_{1,L_C}(\epsilon)|^2$ has two peaks at $\epsilon = \pm\epsilon_B$ with $\epsilon_B \sim W/2 - V/2$ and becomes vanishingly small for $\epsilon < -\epsilon_B$ and $\epsilon > \epsilon_B$, where

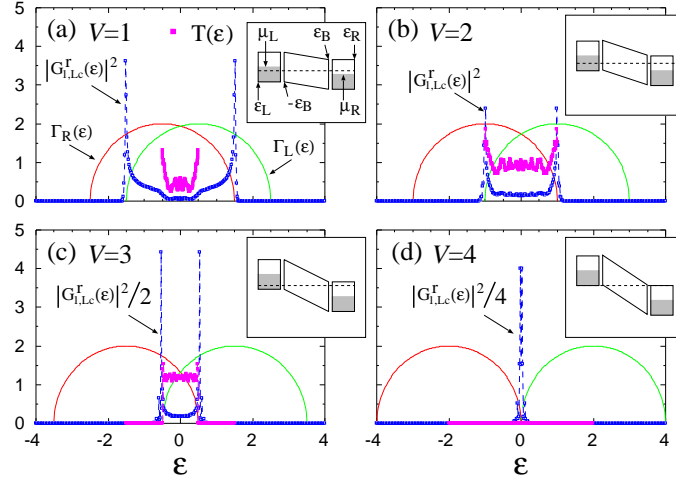


Fig. 3. (Color online) $\Gamma_L(\epsilon)$, $\Gamma_R(\epsilon)$, and $|G_{1,LC}^r(\epsilon)|^2$ as a function of ϵ for several values of V in the case of (i). $T(\epsilon) = \Gamma_L(\epsilon)\Gamma_R(\epsilon)|G_{1,LC}^r(\epsilon)|^2$ is also shown for $\mu_R < \epsilon < \mu_L$. The parameters are the same as those in Fig. 2(b). The inset shows schematic representations of the energy bands of the electrodes and the central part, where the dashed line indicates $\epsilon = 0$.

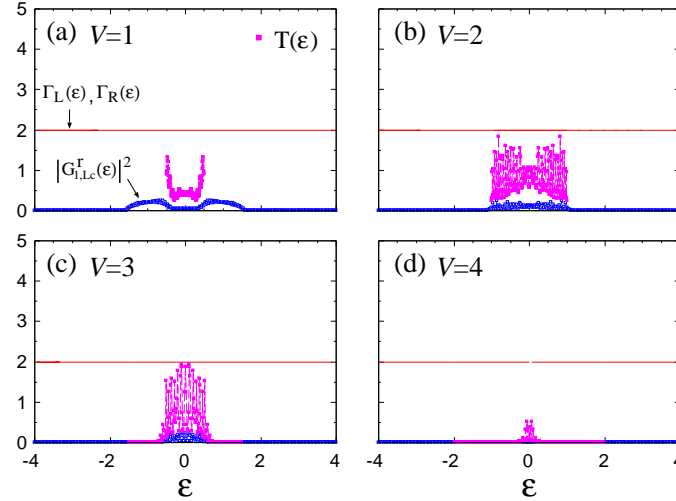


Fig. 4. (Color online) Same plot as in Fig. 3 in the case of (ii).

$W \simeq 4$. We can regard $2\epsilon_B$ as the effective bandwidth for elastic transport because the band is tilted by the potential gradient. This effective bandwidth shrinks with increasing V . For $V < 2$, the regions $\epsilon_L < \epsilon < \epsilon_R$ and $-\epsilon_B < \epsilon < \epsilon_B$ are outside the domain of integration in Eq. (10). In this case, both $\Gamma_L(\epsilon)\Gamma_R(\epsilon)$ and $|G_{1,LC}^r(\epsilon)|^2$ contribute to J , so that J increases with V [Figs. 3(a) and 3(b)]. However, for $V > 2$, these regions come inside the domain $\mu_R < \epsilon < \mu_L$, which results in the NDR [Figs. 3(c) and 3(d)]. The

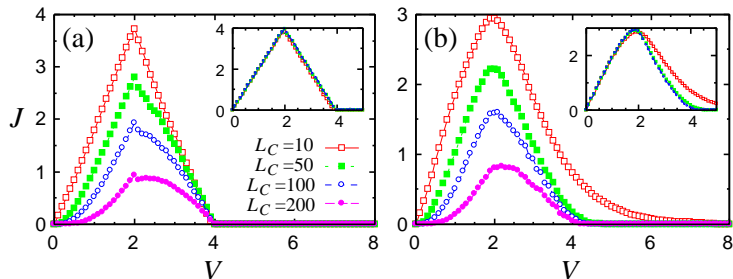


Fig. 5. (Color online) (a) Size dependence of the J - V curve for $\delta t = 0.05$ and $t_E = \tau = 1$ in the case of (i). (b) Same plot in the case of (ii). The inset shows the results for $\delta t = 0$.

onset of the NDR by the finite electrode bandwidth is given by $V = W_E/2$ at which we have $\epsilon_L = \mu_R$ ($\epsilon_R = \mu_L$), whereas that by the potential gradient is given by $V = W/2$ because $\epsilon_B = \mu_L$ ($-\epsilon_B = \mu_R$) holds.

Figure 4 shows the same quantities as in Fig. 3 in the case of (ii). Because of the WBL, $\Gamma_L(\epsilon)$ and $\Gamma_R(\epsilon)$ are independent of ϵ . This indicates that the energy window for the transport, $\epsilon_L < \epsilon < \epsilon_R$, is essentially infinite. Although $|G_{1,L_C}(\epsilon)|^2$ has no sharp peak, its ϵ dependence shows that the effective bandwidth $2\epsilon_B$ decreases with increasing V as in (i). Therefore, the NDR occurs even when we use the WBL. For $V = 1$, $T(\epsilon)$ for $\mu_R < \epsilon < \mu_L$ is similar to that in (i), so that the WBL becomes a good approximation for a small V .¹⁵ In fact, the J - V curves in (i) and (ii) are quantitatively the same for $V < 1.5$, as shown in Fig. 2(b). When we increase V , their difference in $T(\epsilon)$ becomes larger, so that the J - V curve in (ii) deviates from that in (i) for $V > 1.5$. In (iv), the saturation of J is understood from the WBL and $V_C(i)$ in Eq. (6). Since, in this case, $|G_{1,L_C}(\epsilon)|^2$ and $\Gamma_L(\epsilon)\Gamma_R(\epsilon)$ do not depend on V and ϵ , respectively, J becomes constant for $V > W$.

In Figs. 5(a) and 5(b), we show the L_C dependences of the J - V curve in (i) and (ii) for $t_E = \tau = 1$. When L_C is small, J increases almost linearly for small values of V . The tunneling is elastic even when the charge gap exists when the correlation length $\xi = W/\Delta \simeq 20$ is larger than L_C .¹² If we use different values of τ and t_E , stepwise structures in the J - V curve become prominent, which come from the discreteness of the energy spectrum of the central part.¹² As L_C increases, the J - V curve gradually changes into the LZ-type behavior. When $L_C > \xi$, the deformation of the wave function in the central part plays an important role in the breakdown mechanism.¹² Since the threshold for the breakdown is determined by the electric field, $E_{th} \propto \Delta^2/W$, V_{th} is

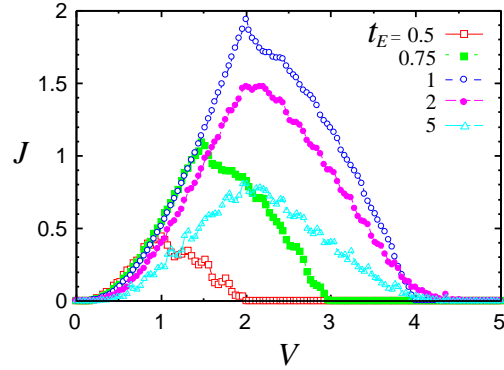


Fig. 6. (Color online) J - V curves for several values of t_E with $\delta t = 0.05$, $\tau = 1$, and $L_C = 100$ in the case of (i).

proportional to L_C . Therefore, J decreases with increasing L_C . The inset shows the results for $\delta t = 0$, which indicates that the size effect is very small when the charge gap is absent. For both the metal and the band insulator, we have $J = 0$ for $V > 4$ in the case of (i) since the overlap between the left and right electrodes disappears [Fig. 3(d)]. In (ii), J is finite even for $V > 4$ owing to the WBL, although it readily approaches zero because the effective bandwidth of the central part vanishes at $V = 4$ [Fig. 4(d)].

In Fig. 6, we show the J - V curves for different values of t_E in (i) with $\delta t = 0.05$, $\tau = 1$, and $L_C = 100$. For $t_E < 1$, the NDR occurs at $V = W_E/2$. This is because for $W_E < W$, the threshold for the NDR by the finite electrode bandwidth is smaller than that by the potential gradient. On the other hand, the NDR sets in at $V = W/2$ for $t_E > 1$ where $W_E > W$ holds. The onset of the NDR is determined by the smaller values of $W/2$ and $W_E/2$.

4. Summary

We have investigated the J - V characteristics of the one-dimensional band insulator attached to electrodes. We have shown that a linear potential gradient and a finite electrode bandwidth cause the NDR, the onsets of which are determined by $V = W/2$ and $V = W_E/2$, respectively. The former effect tilts the energy band of the insulator, so that the NDR results from the shrinkage of the effective bandwidth for elastic transport. Since this mechanism is independent of the electrode degrees of freedom, the NDR occurs even if we use the WBL in contrast to the noninteracting resonant level model.

Acknowledgments

This work was supported by a Grant-in-Aid for Young Scientists (B) (Grant No. 12019365) from the Ministry of Education, Culture, Sports, Science and Technology of Japan.

References

*yasuhiro@phys.chuo-u.ac.jp

- 1) Y. Taguchi, T. Matsumoto, and Y. Tokura, Phys. Rev. B **62**, 7015 (2000).
- 2) S. Yamanouchi, Y. Taguchi, and Y. Tokura, Phys. Rev. Lett. **83**, 5555 (1999).
- 3) T. Mori, I. Terasaki, and H. Mori, J. Mater. Chem. **17**, 4343 (2007).
- 4) K. Yonemitsu, J. Phys. Soc. Jpn. **74**, 2544 (2005).
- 5) T. Oka and N. Nagaosa, Phys. Rev. Lett. **95**, 266403 (2005).
- 6) K. Yonemitsu, N. Maeshima, and T. Hasegawa, Phys. Rev. B **76**, 235118 (2007).
- 7) K. Yonemitsu, J. Phys. Soc. Jpn. **78**, 054705 (2009).
- 8) S. Okamoto, Phys. Rev. B **76**, 035105 (2007).
- 9) S. Okamoto, Phys. Rev. Lett. **101**, 116807 (2008).
- 10) S. Ajisaka, H. Nishimura, S. Tasaki, and I. Terasaki, Prog. Theor. Phys. **121**, 1289 (2009).
- 11) F. Heidrich-Meisner, I. González, K. A. Al-Hassanieh, A. E. Feiguin, M. J. Rozenberg, and E. Dagotto, Phys. Rev. B **82**, 205110 (2010).
- 12) Y. Tanaka and K. Yonemitsu, Phys. Rev. B **83**, 085113 (2011).
- 13) Y. Tanaka and K. Yonemitsu, J. Phys. Soc. Jpn. **80**, 103702 (2011).
- 14) Y. Tanaka and K. Yonemitsu, J. Phys. Condens. Matter **25**, 465603 (2013).
- 15) I. Bâldea and H. Köppel, Phys. Rev. B **81**, 193401 (2010).
- 16) H. Haug and A.-P. Jauho, *Quantum Kinetics in Transport and Optics of Semiconductors* (Springer, Berlin, 2007) 2nd ed.
- 17) A.-P. Jauho, N. S. Wingreen, and Y. Meir, Phys. Rev. B **50**, 5528 (1994).
- 18) L. D. Landau, Phys. Z. Sowjetunion **2**, 46 (1932).
- 19) C. Zener, Proc. R. Soc. London, Ser. A **137**, 696 (1932).